frontiers in Materials

ORIGINAL RESEARCH
published: 11 November 2021
doi: 10.3389/fmats.2021.764928

# High Temperature Chloride Corrosion Behavior of 904L:AlFeNiMoNb High-Entropy Alloy

*Lingyun Bai[1,2], Wenyi Peng[1]*, Dandan Men[2], Jun Zhu[1], Xuecheng Wu[1], Xiongtao Shi[1], Junhuan Xiang[2], Xiaohua Deng[1], Yuqing Wang[1], Zuxiang Sun[1], Siqi Yu[1] and Xiang Wei[1]*

*[1]School of materials science and Engineering, Nanchang University, Nanchang, China, [2]Jiangxi Key Laboratory of Surface Engineering, Jiangxi Science and Technology Normal University, Nanchang, China*

In order to obtain high cost-effective coating materials working in chlorine-containing environment at high temperature, a 904L super austenitic alloy modified by an AlFeNiMoNb alloy (904L:AlFeNiMoNb) was obtained by vacuum arc melting process. The 904L:AlFeNiMoNb high-entropy alloy has a similar phase component with the AlFeNiMoNb alloy, but a more homogenous microstructure than that of the AlFeNiMoNb alloy. High-temperature chloride corrosion tests for 904L, AlFeNiMoNb, and 904L:AlFeNiMoNb high-entropy alloy were carried out under $N_2$–2.6 vol.% $CO_2$–1.3 vol.% $O_2$–2,700 vppm HCl gaseous environment at 700°C and 800°C for 55 h, respectively. Due to the volatilization of $FeCl_2$, weight change curves of the 904L alloy at 700°C and 800°C showed obvious weight loss. Especially at 800°C, the weight loss of the corroded 904L sample was 10 times that of the corroded sample at 700°C. Different from the weight loss situation of the 904L sample, both AlFeNiMoNb and 904L:AlFeNiMoNb high-entropy alloy showed small weight gains under the corrosion temperature of 700°C, while the latter gained half as much weight as the former. When the corrosion temperature was raised to 800°C, the AlFeNiMoNb and 904L:AlFeNiMoNb high-entropy alloy showed flat weight change curves with little weight loss. Weight loss for the AlFeNiMoNb and 904L:AlFeNiMoNb high-entropy alloy were 1.35138 and 0.0118 mg/cm$^2$, respectively. The high temperature chloride corrosion resistance of 904L:AlFeNiMoNb high-entropy alloy is higher than that of 904L and AlFeNiMoNb at both 700°C and 800°C. Meanwhile, on the basis of the morphology and composition results of the corroded samples, combined with thermodynamic calculation, the high-temperature chloride corrosion mechanics of the tested alloys were discussed.

**Keywords: high temperature chloride corrosion, 904L:AlFeNiMoNb highentropy alloy, corrosion kinetics, active oxidation, corrosion mechanics**

OPEN ACCESS

***Edited by:***
*Xin Zhou,*
*Yantai University, China*

***Reviewed by:***
*Himanshu Vashishtha,*
*Indian Institute of Technology Delhi, India*
*Lin Zhou,*
*Donghua University, China*

****Correspondence:***
*Wenyi Peng*
*wenyi.peng@163.com*

***Specialty section:***
*This article was submitted to Polymeric and Composite Materials, a section of the journal Frontiers in Materials*

***Received:*** *26 August 2021*
***Accepted:*** *14 October 2021*
***Published:*** *11 November 2021*

***Citation:***
*Bai L, Peng W, Men D, Zhu J, Wu X, Shi X, Xiang J, Deng X, Wang Y, Sun Z, Yu S and Wei X (2021) High Temperature Chloride Corrosion Behavior of 904L:AlFeNiMoNb High-Entropy Alloy. Front. Mater. 8:764928. doi: 10.3389/fmats.2021.764928*

## INTRODUCTION

Nowadays, more and more municipal wastes are made with the improvement in the living standards of the people and the acceleration of urbanization construction. The proper treatment of municipal waste has become increasingly urgent. At present, the relatively advocated way of waste disposal is incineration technology, which has obvious advantages of environmental protection, energy saving, and reuse of resource (Viklund et al., 2013). However, a lot of corrosive gases, such as HCl, $Cl_2$, and

$SO_2$, will be produced in the process of waste incineration, which will corrode the materials in the incinerator seriously. Among these corrosive gaseous corrosion processes, chlorine-induced high-temperature corrosion results in the most serious failures of materials used in municipal waste incinerators (Zahs et al., 1999). This is because the metal chlorides, which are the corrosion products of alloy matrix under the high-temperature chloride corrosion condition, have low boiling point and high vapor pressure. The volatilization of these corrosion products makes it easier for the base material to be exposed to the corrosive atmosphere, thus, directly accelerating the corrosion progress (Galetz, 2017; Ma et al., 2020). At the same time, the metal oxide obtained by further oxidation of this kind of chloride has relatively loose structure and poor protection performance to the matrix. In order to develop materials with excellent corrosion resistance, chlorine-induced corrosion behavior of alloys has been widely studied (Bender and Schütze, 2003; Galetz et al., 2015; Lequien and Moine, 2018; Izzuddin et al., 2020).

High-temperature chloride corrosion is considered to be an active oxidation process (Viklund et al., 2013; Galetz et al., 2015). Therefore, alloys with excellent high-temperature oxidation resistance might also have a competitive advantage in a high-temperature chloride corrosion environment (Gorr et al., 2017). High-entropy alloys (HEAs), which are composed of various principal components, have a series of characteristics, such as high-entropy effect, lattice distortion effect, sluggish diffusion effect, and cocktail effect, which make them possess high tensile strength, high hardness, high wear resistance, and high corrosion resistance (Tsao et al., 2016). In the past decades, HEAs have been widely studied in the high-temperature oxidation and electrochemical corrosion area. Under high concentrations of sulfuric acid, hydrochloric acid, nitric acid, and other corrosive solution condition, HEAs show excellent localized and general corrosion resistance. The addition of Al, Cr, Ni, Nb, Ti, and Mo can make a passive film on the coating surface (Zhang et al., 2018; Izzuddin et al., 2020). The addition of Mo can form a self-healing passive film with Cr, which can effectively inhibit the pitting corrosion caused by the Cl ion (JIA Chuntang. Research, 2019). On the other hand, Mo might promote the enrichment of Cr in the formed protective layer and consequently enhance the corrosion resistance of the coating (Sadeghi and Joshi, 2019). However, the high-temperature corrosion of HEAs in a chlorine-containing atmosphere, which is similar to the conditions of waste incineration, is rarely reported, and the existing research mainly focused on the hot corrosion of HEAs (Li et al., 2021).

Nowadays, Ni-based alloy, such as Inconel625 alloy is often used as a protective weld overlay material used on the inner surface of the waste incinerator. As reported in many studies, Inconel625 alloy exhibits high corrosion resistance in waste-to-energy plants (Fantozzi et al., 2017; Pooja et al., 2021). However, the high price of Inconel625 limits its wide application in practical production. Meanwhile, the kinds of alloy or coating materials that can be used in a high-temperature chloride corrosion environment are very limited; the Ni-based alloys, such as Inconel625 and C276, are the main ones in waste incinerators (Pooja et al., 2021).

Super-austenitic stainless steel (SASS) 904L, which is a kind of Fe-based alloy, has a much lower price than that of the Ni-based alloy. 904L is highly resistant toward pitting, crevice, and chloride stress corrosion due to the presence of high concentrations of Cr, Ni, and Mo (Devendranath Ramkumar et al., 2016a; Wang et al., 2021). Compared with ordinary austenitic stainless steel, 904L is not only highly alloyed but also has a particularly low impurity content. Therefore, 904L has higher corrosion resistance than that of a traditional stainless steel in acidic environments. 904L is expected to become a substitute for nickel-based alloy in a high-temperature corrosion environment, but there is little research on its corrosion performance, especially in high-temperature chloride corrosion environment. A previous study shows that the addition of Mo-rich Ni-based metals could improve the pitting corrosion resistance of 904L (Devendranath Ramkumar et al., 2016b).

The purpose of this study is to reduce the cost of the protective coating materials used in high-temperature chloride corrosion environment and expand the selection range of corrosion-resistant coating materials. Combined with the low price and excellent corrosion characteristics of 904L in a corrosive environment and the advantages of high-entropy alloy in high temperature oxidation field, in this research, an AlFeNiMoNb-modified 904L alloy (904L:AlFeNiMoNb) was prepared, and the chloride corrosion properties at the temperatures of 700°C and 800°C of 904L, AlFeNiMoNb, and 904L:AlFeNiMoNb alloy were investigated.

## MATERIALS AND EXPERIMENTAL METHOD

### Materials

High-purity (99.99%) Al, Fe, Ni, Mo, and Nb powders with the same molar ratio of each element were invoked as raw materials to prepare an AlFeNiMoNb plate by hot pressing technology.

To improve the high-temperature chloride corrosion resistance of 904L and lower the cost of AlFeNiMoNb alloy, 904L:AlFeNiMoNb high-entropy alloy was obtained by mixing a commercial 904L plate and an AlFeNiMoNb plate with an equimolar ratio by arc melting process. At last, the as-cast 904L:AlFeNiMoNb high-entropy alloy was annealed at 900°C for 24 h to homogenize its composition. The actual chemical compositions of the 904L, AlFeNiMoNb, and 904L:AlFeNiMoNb alloys detected by energy dispersive spectroscopy (EDS) analysis

**TABLE 1 |** The actual composition of the test samples detected by energy dispersive spectroscopy (EDS) technology.

| Component (at%) sample | Al | Fe | Ni | Mo | Nb | Cr | Cu |
|---|---|---|---|---|---|---|---|
| AlFeNiMoNb | 20.18 | 19.17 | 20.99 | 19.11 | 20.00 | 0 | 0 |
| 904L | 0 | 50.00 | 23.78 | 3.06 | 0 | 21.66 | 1.5 |
| 904L:AlFeNiMoNb | 9.54 | 35.38 | 21.46 | 12.26 | 9.17 | 11.63 | 0.57 |

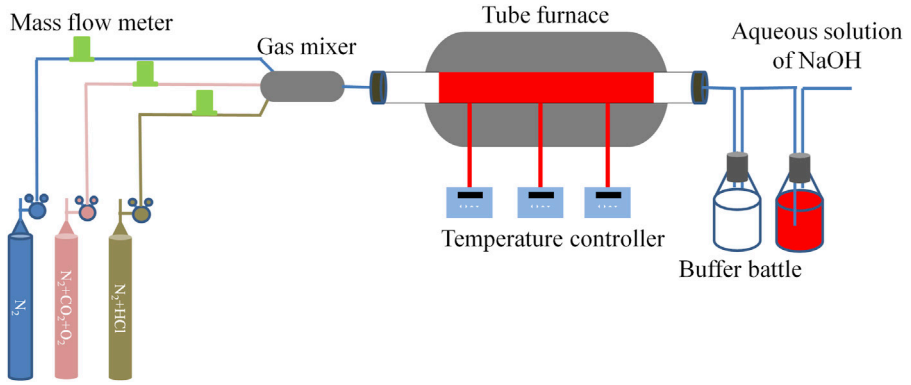


**FIGURE 1 |** Test device of the high-temperature chloride corrosion.

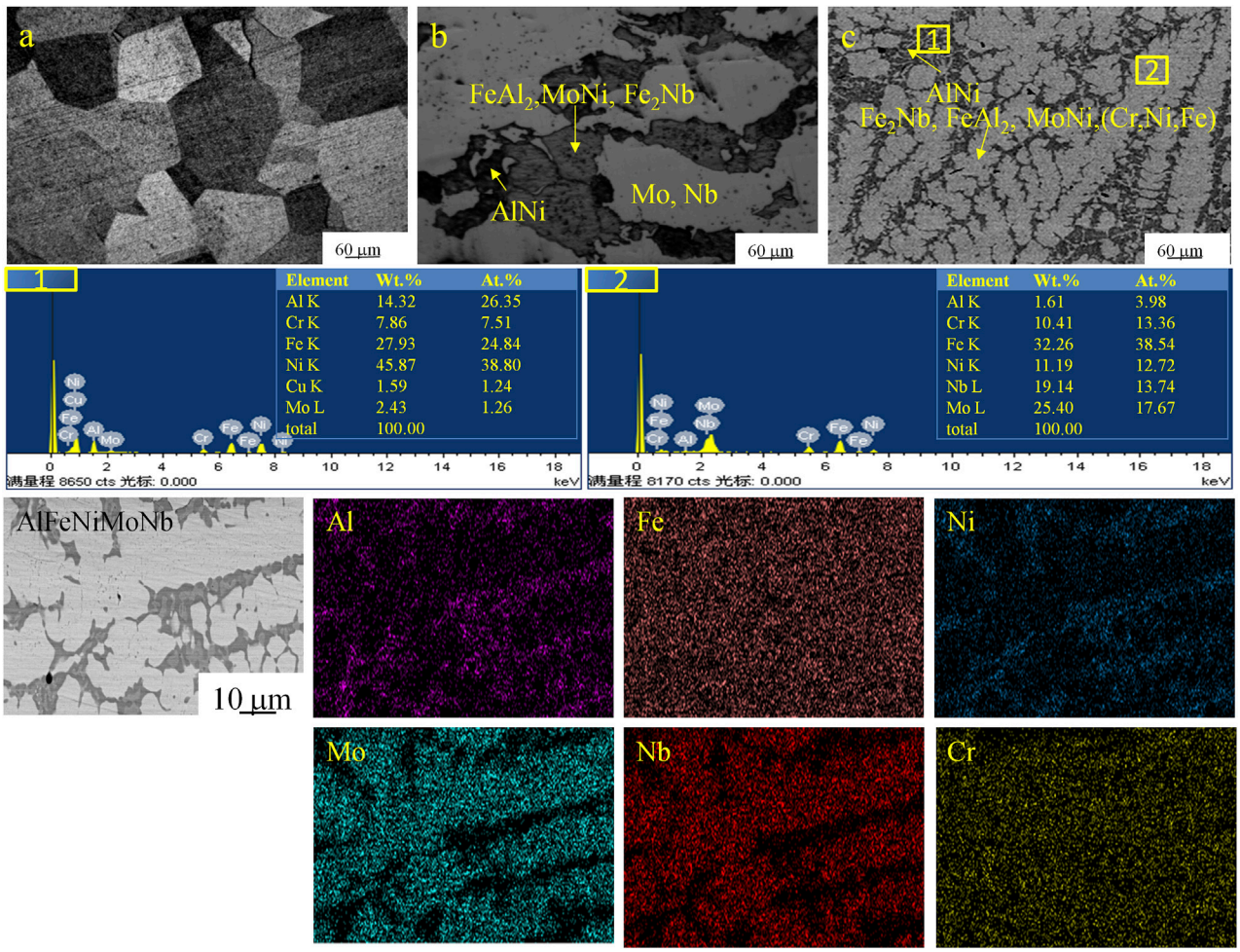


**FIGURE 2 |** Metallographic pictures of the tested alloys and energy dispersive spectroscopy (EDS) results of 904L:AlFeNiMoNb. **(A)**: 904L; **(B)**: AlFeNiMoNb; **(C)**: 904L:AlFeNiMoNb.

are shown in **Table 1**. In order to investigate the corrosion performance, the tested alloys were cut into pieces with the size of 10 × 5 × 2.5 $mm^3$ by a wire-cutting equipment (WEDM).

## Corrosion Test

Corrosion tests were carried out under $N_2$–2.6 vol.% $CO_2$–1.3 vol.% $O_2$–2,700 vppm HCl gaseous environment at 700°C and

800°C for 55 h, respectively. Each specimen was placed into a single quartz crucible, so that any spallation of corrosion products could be collected separately after exposure. Then all the samples were placed into the silica tube of a horizontal tube furnace, which had three temperature control instruments to ensure the uniformity of temperature in the furnace as shown in **Figure 1**. Only $N_2$ and the mixture of $N_2$, $CO_2$, and $O_2$ were input at the temperature-rising stage, which had a heating rate of 4°C/min. The flow rate of each gas was controlled by a mass flow meter. After mixing in the chamber, gases were input into the silica tube. When the temperature reached 700°C, the mixture of HCl and $N_2$ was input into the corrosion system. The total flow of all gases was 75 ml/min. At the end of the gas path, excessive HCl was absorbed by NaOH aqueous solution. The corrosion kinetics of the samples were obtained by the gravimetric method. The corrosion process was stopped every 5 h. Samples were cooled naturally with the furnace, and then an electronic balance, with a precision of 1 in 100,000, was utilized to weigh the samples. After that, the corrosion process was carried on until 55 h.

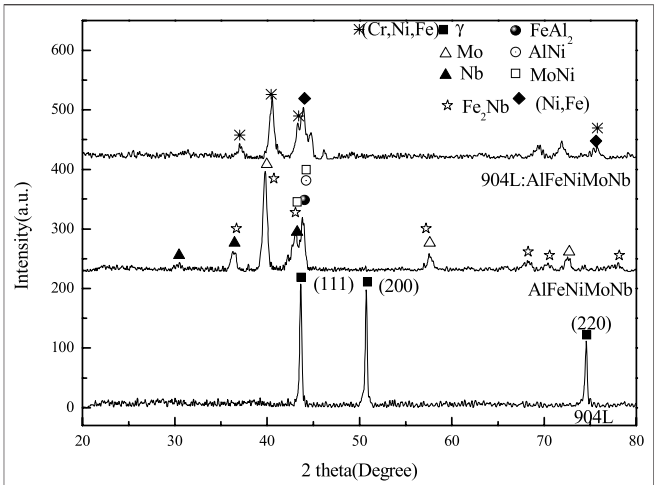


**FIGURE 3 |** X-ray diffraction patterns of the obtained alloys before corrosion test.

## Analysis Methods

In order to examine the microstructure and composition of the experimental samples, metallographic method, scanning electron microscopy (SEM), energy dispersive spectroscopy (EDS), and x-ray diffraction (XRD) detections were used before the corrosion process. After the corrosion experiments, the morphology and composition of the surface and cross-section of the specimens were examined using SEM/EDS and XRD technology. The analysis of the cross-section morphology of the scales was undertaken by molding the corroded samples in resin, and metallographic sections were prepared. The cross sections were ground and polished dry to prevent dissolution of the formed chlorides.

# RESULTS AND DISCUSSIONS

## Structure of the Obtained Alloys

The metallographic diagrams of 904L, AlFeNiMoNb plate, and 904L: AlFeNiMoNb high-entropy alloy and the EDS results of 904L: AlFeNiMoNb are presented in **Figure 2**. 904L had a typical austenite structure. The AlFeNiMoNb plate had several different phase compositions as shown in **Figure 3**, which were obtained by the analysis of its XRD and EDS results. The bright region in the metallographic diagram of the alloy was the Mo-rich phase, which contained part of Nb. The gray region contained many phases, just like $FeAl_2$, MoNi, and $Fe_2Nb$. In the black portion, AlNi was dominant. Compared with 904L and AlFeNiMoNb alloys, 904L: AlFeNiMoNb had a rather homogeneous and refined microstructure (**Figure 2C**). The 904L:AlFeNiMoNb alloy has a dendrite microstructure. The dendrites were mainly composed of AlNi and (Ni, Fe) solid solutions, while the composition between dendrites were mainly composed of (Cr, Ni, and Fe) and (Ni, Fe) solid solutions and other intermetallic compounds, such as $Fe_2Nb$, $FeAl_2$, and MoNi.

From the XRD patterns of the obtained alloys, it could be analyzed that the 904L:AlFeNiMoNb alloy had a similar phase composition with the AlFeNiMoNb alloy, but there was no obvious Mo diffraction peaks detected. Meanwhile, diffraction peaks of (Cr, Ni, and Fe) and (Ni, Fe) solid solutions became more obvious. These results were consistent with the metallographic diagrams of the alloys; the melting process of the 904L alloy and AlFeNiMoNb alloy promoted the homogenization of microstructure and simplification of phase composition. From the composition of the 904L:AlFeNiMoNb, it could be seen that there were more than five elements, whose concentration were in the range of 5–35 at%. Combined with the XRD analysis of the obtained alloy, 904L: AlFeNiMoNb could be considered as a kind of high-entropy alloy and might have excellent corrosion resistance.

## High-Temperature Chloride Corrosion Process

From the perspective of thermodynamics, the driving force of chemical reaction is the change value of Gibbs free energy in the reaction process. The more negative the value, the greater the driving force of the reaction, and the more likely the reaction is to occur.

**Figure 4** shows the temperature dependence of Gibbs free energy of metal oxidation and chlorination calculated by HSC6.0.

As far as the same metal was concerned, the Gibbs free energy changes in the reaction between metal and $O_2$ to obtain metal oxide ($M_xO_y$) and the reaction among metal, HCl, and $O_2$ to obtain chloride oxide of metal ($MO_xCl_y$) are similar. So, at the initial stage of the process of high-temperature chloride corrosion, the metals were oxidized to $M_xO_y$ and $MO_xCl_y$ easily, and the formation of $MCl_x$ was not competitive. $MCl_x$ and $MO_xCl_y$ products are unstable phases under the experimental temperature, and have low melting point and high equilibrium vapor pressure. They will volatilize outward from the interface between alloy matrix and the corrosion layer to the surface of the corroded sample. With the increase in the oxygen pressure during this diffusion path, $MCl_x$ and $MO_xCl_y$ will be oxidized to metal oxides or leave the sample surface with the carrier gas, and the latter process could cause the mass loss of the tested sample during the corrosion process.

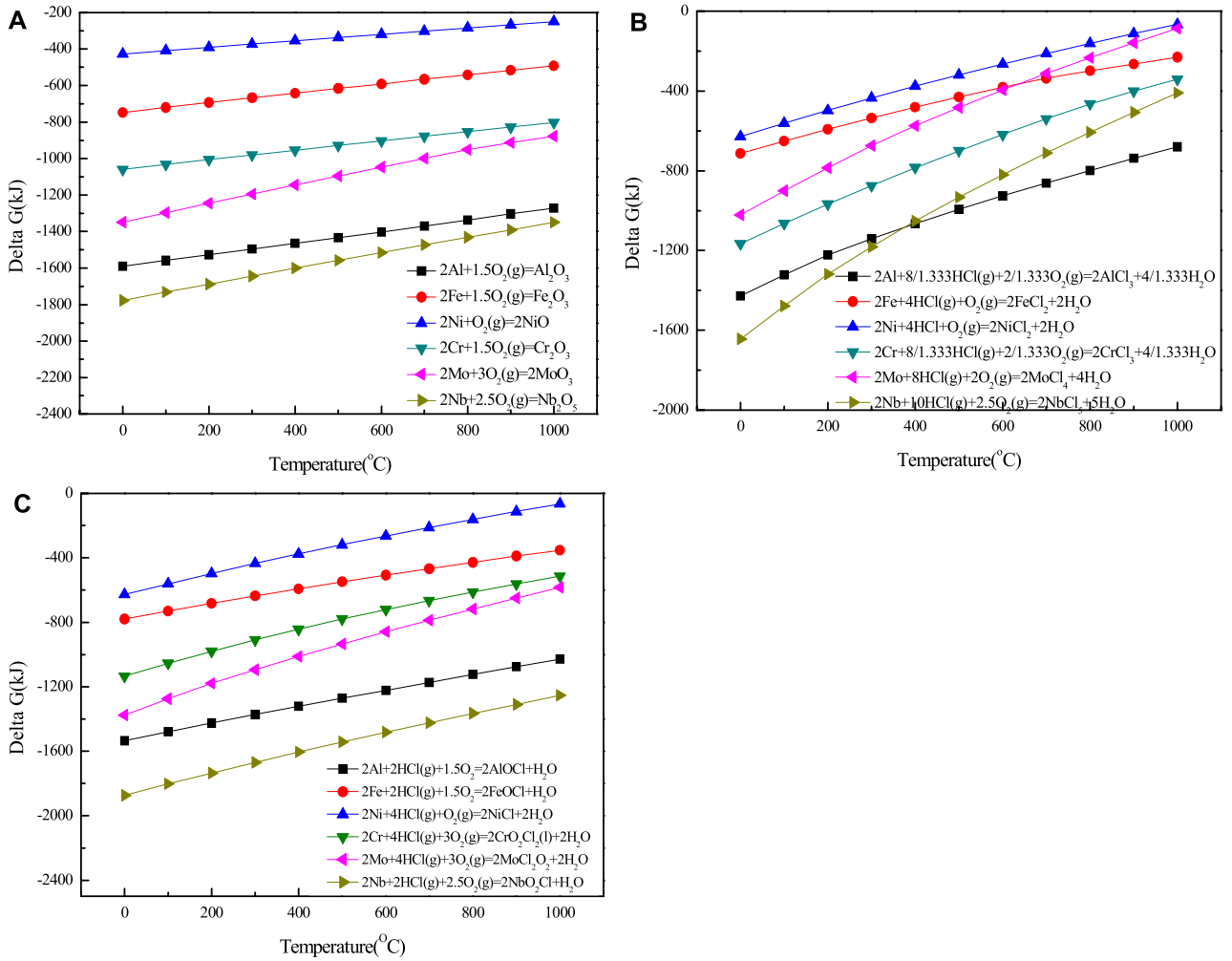


**FIGURE 4 |** Temperature dependence of Gibbs free energy of metal oxidation and chlorination calculated by HSC6.0 **(A)** M + $O_2$(g) = MxOy; **(B)** M + HCl(g) + $O_2$(g) = $MCl_x$ + $H_2O$; **(C)** M + HCl(g) + $O_2$(g) = $MO_xCl_y$ + $H_2O$.

The difficulty of oxidation of $MCl_x$ and $MO_xCl_y$ to metal oxides is related to the driving force of oxidation reaction, that is, the change in Gibbs free energy of the reaction between these compounds and oxygen. **Figure 5** shows the temperature dependence of Gibbs free energy of oxidation reaction of $MCl_x$ and $MO_xCl_y$ calculated by HSC6.0. $MCl_x$ and $MO_xCl_y$ will be oxidized to $M_xO_y$, and $Cl_2$ is released. These kinds of oxides, which are obtained by gas reaction, are very loose and have no effective protection of the metal matrix from the corrosive media of $Cl^-$ (Li, 2000). Due to the existence of chloride concentration gradient, the generated $Cl_2$ will diffuse back to the corrosion layer/metal interface and continue to corrode the metal matrix. On the outer surface of the corrosion layer, the corrosive HCl will react with the formed oxides to obtain $MCl_x$. Therefore, what needs to be investigated next is the stability of metal oxides in the chlorine atmosphere, which could be evaluated by the driving force of the chemical reaction between metal oxide and HCl.

**Figure 6** shows the temperature dependence of Gibbs free energy for the reaction of metal oxides with HCl calculated by HSC6.0. The higher the Gibbs free energy, the more stable the metal oxide is. On the basis of thermodynamic calculation, the high-temperature chloride corrosion process can be described by **Figure 7**; the corresponding process has been described above.

## High-Temperature Chloride Corrosion Kinetics

**Figure 8** shows thermo-gravimetric results for the high-temperature chloride corrosion of alloys at 700°C and 800°C for 55 h under $N_2$–2.6 vol.% $CO_2$–1.3 vol.% $O_2$–2,700 vppm HCl gaseous environment. When the corrosion temperature was 700°C, 904L showed obvious mass loss, especially after being corroded for 10 h. On the other hand, AlFeNiMoNb and 904L: AlFeNiMoNb high-entropy alloy showed mass gain. After being corroded for 55 h, the total mass gain of 904L, AlFeNiMoNb

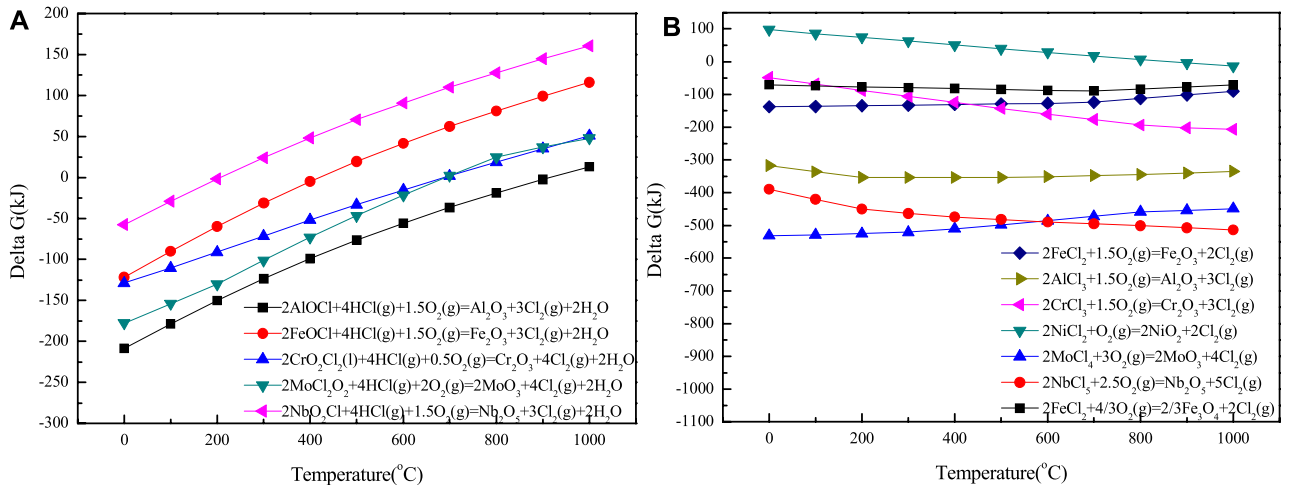


**FIGURE 5 |** Temperature dependence of Gibbs free energy of oxidation reaction of MClx and MOxCly calculated by HSC6.0: **(A)** for MOxCly; **(B)** for MClx.

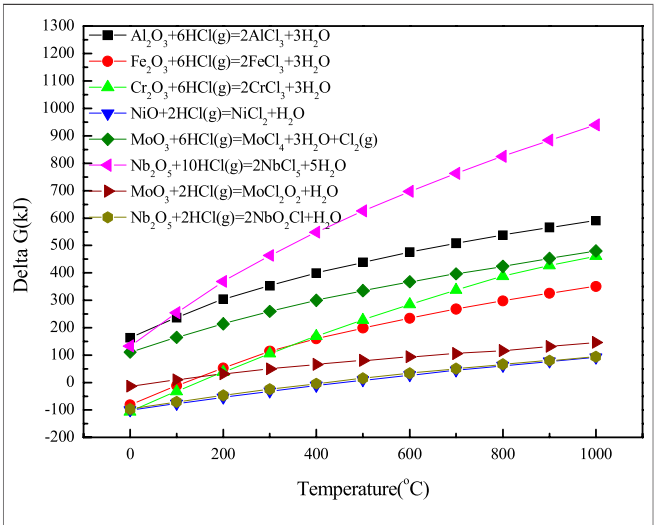


**FIGURE 6 |** Temperature dependence of Gibbs free energy for the reaction between metal oxides and HCl calculated by HSC6.0.

plate, and 904L:AlFeNiMoNb high-entropy alloy was −3.09557, 0.30425, and 0.15714 mg/cm$^2$, respectively. With the corrosion temperature increasing to 800°C, 904L showed serious mass loss during the chloride corrosion process, especially at the time range of 10–25 h. After 25 h, the thermo-gravimetric curve of 904L showed a relatively slight change in mass. Both AlFeNiMoNb plate and 904L:AlFeNiMoNb high-entropy alloy showed almost straight thermo-gravimetric curves with small mass changes, especially for the latter. After being corroded for 55 h, 904L, AlFeNiMoNb plate, and 904L: AlFeNiMoNb high-entropy alloy obtained a total mass gain of −33.36776, −1.35138, and −0.0118 mg/cm$^2$, respectively.

From the thermo-gravimetric data for the high-temperature chloride corrosion process of the tested alloys, it could be concluded that the 904L alloy was not suitable for the application in oxidizing chlorine-containing atmosphere above 700°C. On the other hand, the AlFeNiMoNb plate and 904L: AlFeNiMoNb high-entropy alloy showed excellent corrosion resistance under the corrosion temperatures of 700°C and 800°C. The 904L:AlFeNiMoNb high-entropy alloy had the highest high-temperature chloride corrosion resistance among the samples and also had the most stable corrosion resistance with the change in temperature.

The corrosion properties of materials are closely related to their composition and microstructure. From the temperature dependence of Gibbs free energy of metal oxidation and chlorination as shown in **Figure 4**, it could be concluded that the Ni element has the highest Gibbs free energy change among the selected elements during the reaction of oxidation and chlorination. This result means that Ni has excellent high-temperature chloride corrosion resistance and could be chosen as the main composition of the matrix alloy. From **Figures 5**, **6**, it could be analyzed that $Al_2O_3$ was the corrosion product with the most stable properties under the oxidizing atmosphere containing chlorine. The formation of $Al_2O_3$ products can effectively prevent the further corrosion of chlorine to matrix elements.

There was no Al element in the 904L sample, which had the highest corrosion resistance under the test environment. At the same time, 904L also had the highest Fe concentration, whose chlorination product $FeCl_2$ had very high equilibrium vapor pressure. As a result, when the corroded temperature was higher than 700°C, 904L showed significant mass loss and showed the poorest high-temperature chloride corrosion resistance.

From the temperature dependence of Gibbs free energy of metal oxidation (**Figure 4**), it could be seen that oxidations of Al, Nb, and Mo elements have low Gibbs free energy change during the oxidation reaction, so they would be oxidized easily, and the process will cause mass gain of the sample. The AlFeNiMoNb plate had higher concentrations of Al, Nb, and Mo than that of 904L:AlFeNiMoNb high-entropy alloy. As a result, the AlFeNiMoNb plate should obtain a higher mass gain than that of 904L:AlFeNiMoNb high-entropy alloy. In fact, when the

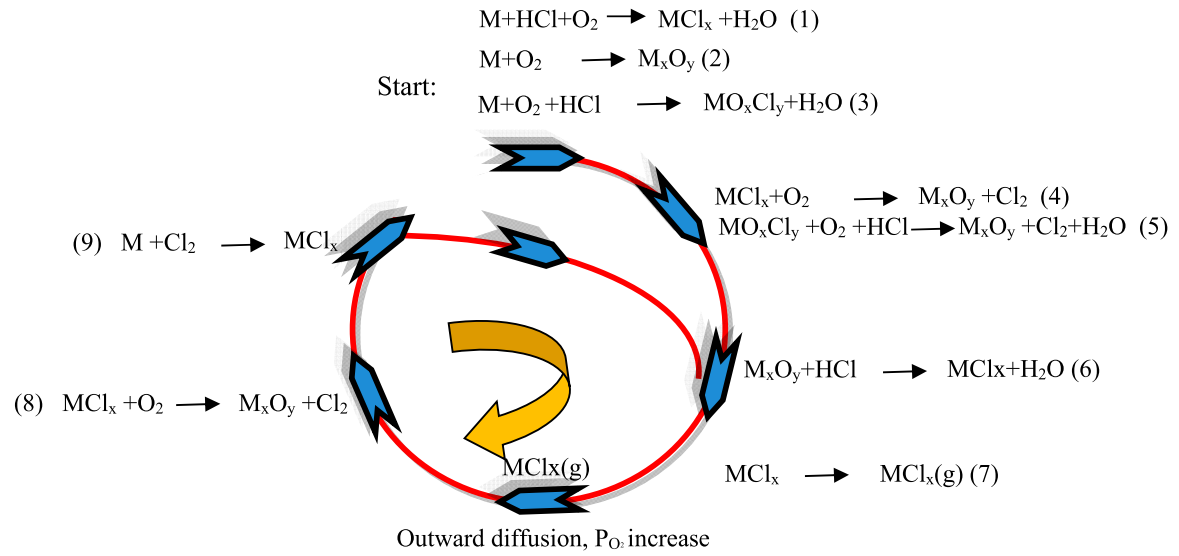


**FIGURE 7 |** High-temperature chloride corrosion process of metals.

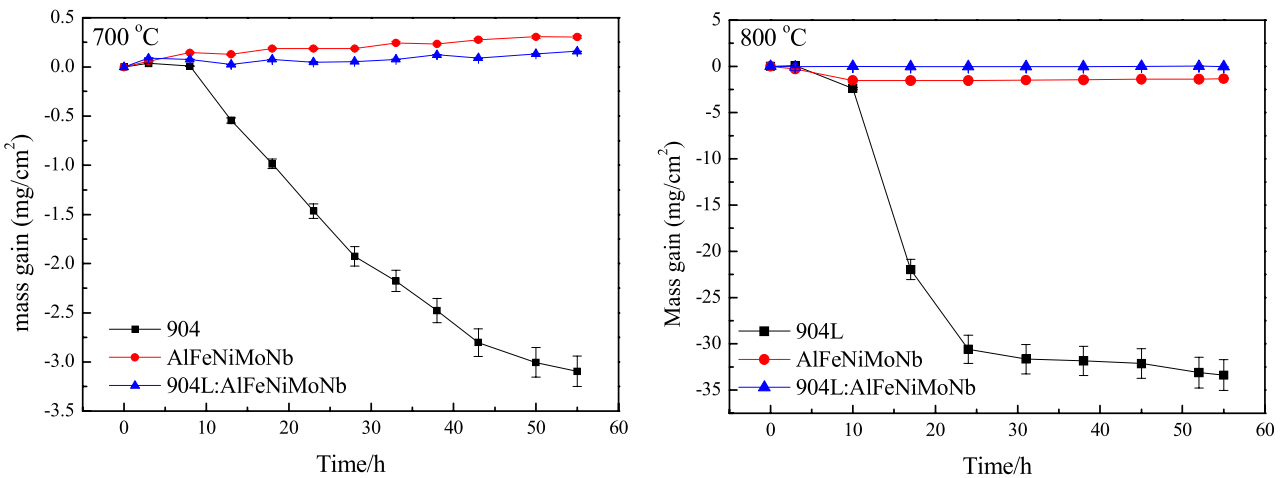


**FIGURE 8 |** Thermo-gravimetric results for the high-temperature chloride corrosion of alloys at 700°C and 800°C for 55 h under $N_2$–2.6 vol.% $CO_2$–1.3 vol.% $O_2$–2,700 vppm HCl gaseous environment.

corrosion temperature was 700°C, experimental result was consistent with the above analysis, but when the corrosion temperature was increased to 800°C, the AlFeNiMoNb plate showed mass loss. This phenomenon was caused by the fact that at a higher temperature, the volatilization of metal chlorides with high vapor pressure was dominant, especially for the AlFeNiMoNb plate, which had numerous phase boundaries. The phase boundary may still be the main position of discontinuity during the formation of corrosion layer. Therefore, a large number of phase boundaries led to the existence of many defects in the corrosion layer and became fast channels for chloride volatilization. Finally, the weight loss of the material appeared in the process of high-temperature chloride corrosion.

The 904L:AlFeNiMoNb high-entropy alloy had a rather homogeneous and refined microstructure (**Figure 2C**). This structure was conducive to the uniform corrosion process and the formation of continuous protective oxide film. Therefore, the high-entropy alloy showed the best corrosion resistance under experimental conditions.

## Surface Morphology and Composition of the Corroded Samples

**Figure 9** shows the x-ray diffraction patterns of the corroded surface of alloys after high-temperature chloride corrosion at 700°C and 800°C for 55 h. **Figure 10** shows the surface

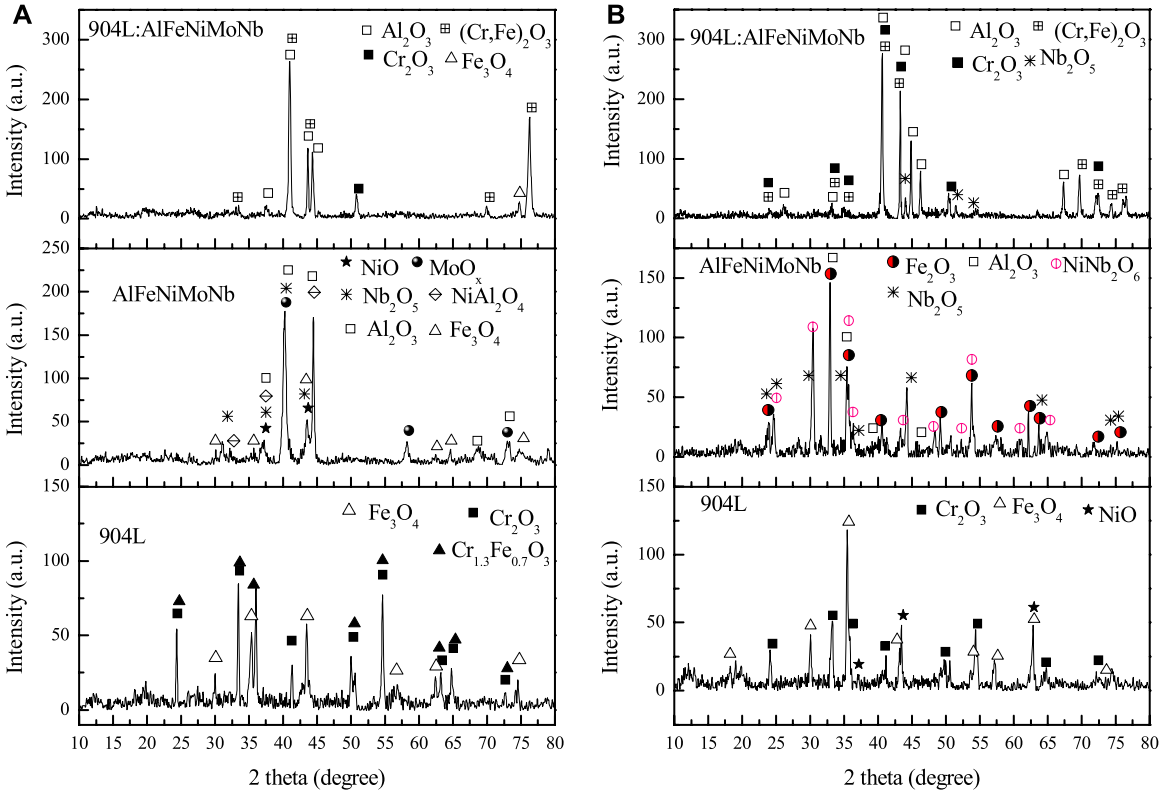


**FIGURE 9 |** X-ray diffraction patterns of the corroded surfaces of alloys after high temperature chloride corrosion at 700°C and 800°C for 55 h under $N_2$–2.6 vol.% $CO_2$–1.3 vol.% $O_2$-2,700 vppm HCl gaseous environment [**(A)** for 700°C; **(B)** for 800°C].

morphology and composition of alloys after high-temperature chloride corrosion at 700°C and 800°C for 55 h.

When the corrosion temperature was 700°C, the surface of the 904L sample was mainly composed of $Cr_2O_3$ (PDF#38-1479), $Cr_{1.3}Fe_{0.7}O_3$ (PDF#35-1112), and $Fe_3O_4$ (PDF#28-0491). After corrosion, the surface of the AlFeNiMoNb sample was mainly composed of $Al_2O_3$ (PDF#11-0517), $Nb_2O_5$ (PDF#12-0104), NiO (PDF#89-7390), $NiAl_2O_4$ (PDF#10-0339), $MoO_x$ (PDF#21-0569, PDF#32-0671), and $Fe_3O_4$ (PDF#26-1136). For the 904L:AlFeNiMoNb high-entropy alloy, the surface after corrosion was mainly composed of $Al_2O_3$ (PDF#10-0173, PDF#13-1373), $(Cr,Fe)_2O_3$ (PDF#02-1357), $Cr_2O_3$ (PDF#38-1479), and $Fe_3O_4$ (PDF#26-1136). Compared with the AlFeNiMoNb plate, there was little corrosion products containing Ni on the surface of the 904L:AlFeNiMoNb high-entropy alloy. The results can be analyzed by the difference in microstructure between the two alloys. As shown in the metallographic structure picture of alloys (**Figure 2**), different phases of AlFeNiMoNb alloy were clearly distinguished (**Figure 2B**), and each phase occupied a certain area. Ni was mainly concentrated in dark and gray areas, and existed in the form of AlNi and MoNi. After the corrosion of the sample, the corrosion products of Ni elements in these areas, such as NiO, can be detected. Although the 904L:AlFeNiMoNb high-entropy alloy had a similar Ni concentration as the 904L, it has a homogenous microstructure (**Figure 2C**), and the dispersion of Ni was more uniform. It can be seen from the calculation results of Gibbs free energy change of element oxidation and chlorination reaction in **Figure 4** that the oxidation and chlorination reaction of Ni has a smaller driving force than that of other elements, that is, during the corrosion process, Al, Cr, and Fe elements were oxidized quickly than Ni, and at last, $Al_2O_3$, $(Cr,Fe)_2O_3$, $Cr_2O_3$, and $Fe_3O_4$ products covered the corrosion surface of the sample. On the other hand, from the actual chemical composition of the tested samples, which are shown in **Table 1**, it could be seen that there was 11.63 at % Cr in the 904L:AlFeNiMoNb high-entropy alloy, which was absent in the AlFeNiMoNb alloy. **Figure 4** shows that the driving force for the oxidation reaction of Cr is much higher than that of Ni, so $Cr_2O_3$ is more likely to be formed on the surface of the sample from the perspective of thermodynamics. Meanwhile, the equilibrium vapor pressure of $CrCl_3$ (**Figure 11**) is higher than that of $NiCl_2$, and the partial pressures of oxygen required for the oxidation reaction of $CrCl_3$ to $Cr_2O_3$ (**Figure 12**) are lower than that of $NiCl_2$ at the temperatures of 700°C and 800°C, which indicated that the Cr element in the alloy matrix could diffuse outward easily than Ni and eventually formed $Cr_2O_3$ on the surface of the sample, as shown in **Figures 9**, **10**. As a result, Ni is forming oxides on the surface of AlFeNiMoNb only, but there is no sign of NiO in 904L:AlFeNiMoNb.

When the corrosion temperature was raised to 800°C, the content of $Fe_3O_4$ in the corrosion product of 904L increased, while the content of $Cr_2O_3$ decreased. At the same time, the

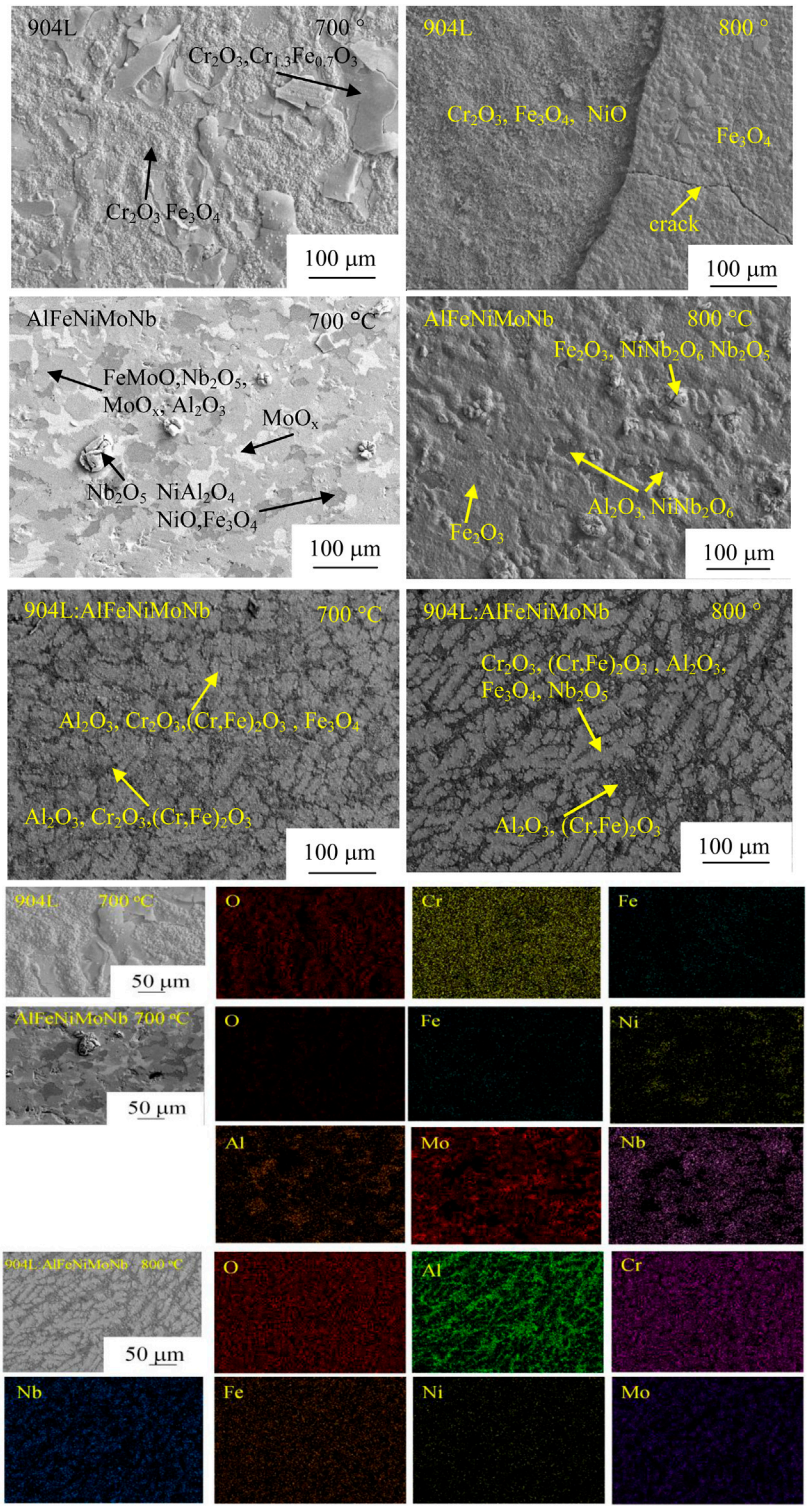


**FIGURE 10 |** Surface morphology and composition of alloys after high-temperature chloride corrosion at 700°C and 800°C for 55 h under $N_2$–2.6 vol.% $CO_2$–1.3 vol.% $O_2$–2,700 vppm HCl gaseous environment.

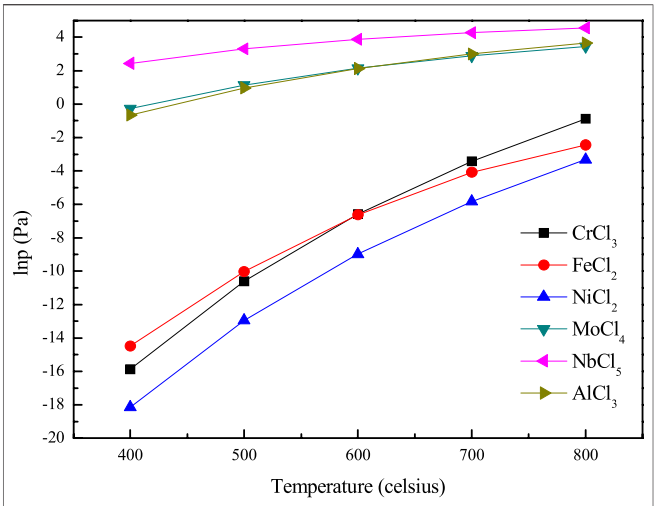


**FIGURE 11 |** Equilibrium vapor pressures of solid chlorides at 400–800°C calculated by HSC6.0.

diffraction peaks of NiO appeared. Cr could be oxidized easily to form $Cr_2O_3$ than Fe to form oxide of ion (**Figure 4A**), and $Cr_2O_3$ was more stable than iron oxide under the corrosion condition (**Figure 6**). As a result, when the corrosion temperature was 700°C, there were more $Cr_2O_3$ on the surface of 904L after corrosion. At the same time, from the equilibrium vapor pressures of solid chlorides at 400–800°C (**Figure 11**), it could be seen that the equilibrium vapor pressure of $CrCl_3$ was slightly higher than that of $FeCl_2$ at 700°C. From the oxygen pressure required for the oxidation of metal chlorides to metal oxides (**Figure 12**), it can be seen that the oxygen partial pressure required for the oxidation of $CrCl_3$ is significantly lower than that of $FeCl_2$ at 700–800°C. Therefore, the rapidly evaporated $CrCl_3$ was quickly oxidized to $Cr_2O_3$ on the surface, resulting in a higher content of chromium oxide on the 904L surface than iron oxide at 700°C. When the corrosion temperature was raised, the corrosion of the alloy became serious, and the thickness of the corrosion layer increased. As can be seen in **Figure 12**, the oxygen partial pressure required for the oxidation of $FeCl_2$ to oxide is higher than that for $CrCl_3$. Therefore, iron oxides tended to be formed on the surface of the corrosion layer closer to the gas phase where the partial pressure of oxygen was higher than the inner side of the corrosion layer. Therefore, the preferentially grown $Cr_2O_3$ was covered by the subsequently formed iron oxides. The theoretical analysis was in good agreement with the experimental results. On the other hand, the thick corrosion layer with poor adhesion to the substrate was prone to rupture during the cyclic corrosion process with the temperature increasing and decreasing, resulting in the exposure of corrosion products of the inner layer, such as NiO, as shown in the surface morphology and composition of 904L after corroded at 800°C for 55 h in **Figure 10**.

For the AlFeNiMoNb plate, the iron oxide changed from $Fe_3O_4$ to $Fe_2O_3$ with the corrosion temperature increased from 700°C to 800°C. The NiO, Mo oxides, and $NiAl_2O_4$ in the products were not obvious any more. Instead, the products of $NiNb_2O_6$ appeared. After corrosion at 700°C, the surface of the sample was composed of oxides of many elements. The driving forces of Al, Nb, and Cr that reacted with oxygen were greater than that of Fe (**Figure 4A**). As a result, the oxygen partial pressure left for Fe oxidation was small. It can be seen from the predominance diagram for the Fe–O–Cl system in **Figure 13** that when the oxygen partial pressure is low, it is conducive to the formation of $Fe_3O_4$. When the corrosion temperature was raised to 800°C, the corrosion degree increased, and the corrosion layer thickened. The vapor pressure of unstable iron chloride is very high (**Figure 11**), and the oxygen partial pressure required for the oxidation of iron chloride is high too (**Figure 12**). Therefore, the surface of the corrosion layer was mainly iron oxide. Because there was no competition for oxidation of other elements at this time, the oxygen partial pressure for Fe oxidation was high, which was conducive to the formation of $Fe_2O_3$.

As far as the 904L:AlFeNiMoNb high-entropy alloy was concerned, the corrosion products at 800°C were mainly composed of $(Cr,Fe)_2O_3$, $Al_2O_3$, $Cr_2O_3$, and a small amount of $Nb_2O_5$. Compared with corrosion at 700°C, the content of $(Cr,Fe)_2O_3$ was significantly improved. The diffraction peak of $Fe_3O_4$ among the corrosion products was not obvious at the corrosion temperature of 800°C. The corrosion product of the high-entropy alloy had good stability in the high-temperature corrosion environment containing chlorine. Therefore, it effectively prevented the further corrosion of Cl to the alloy matrix and inhibited the formation and volatilization of unstable iron chloride. Therefore, no iron oxide was detected on the alloy surface after corrosion.

**Figure 13** shows the thermodynamic stability diagrams of the systems of Fe–O–Cl, Al–O–Cl, Ni–O–Cl, Mo–O–Cl, Nb–O–Cl, and Cr–O–Cl at 800°C, which were calculated by HSC6.0. These results can help researchers to predict corrosion products and corrosion process. The partial pressure of $O_2$ and HCl in this study was 0.01315 and 0.0027, respectively, which had been marked with "*" in the pictures. Under these conditions, the

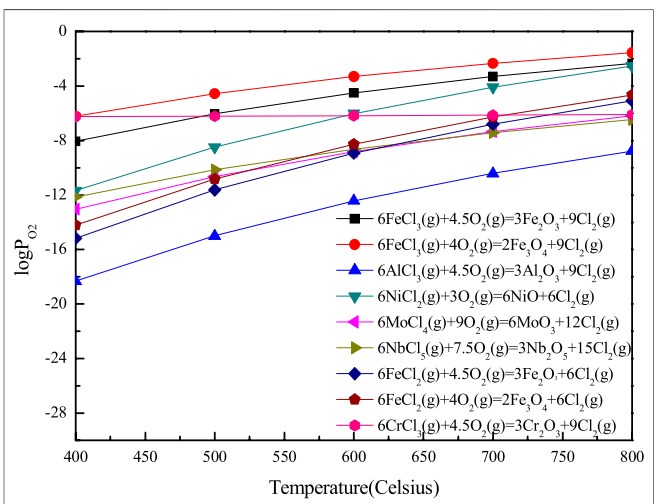


**FIGURE 12 |** Partial pressure of oxygen required for oxidation of metal chlorides to metal oxides at 400–800°C calculated by combination of Van't Hoff isothermal equation and HSC6.0.

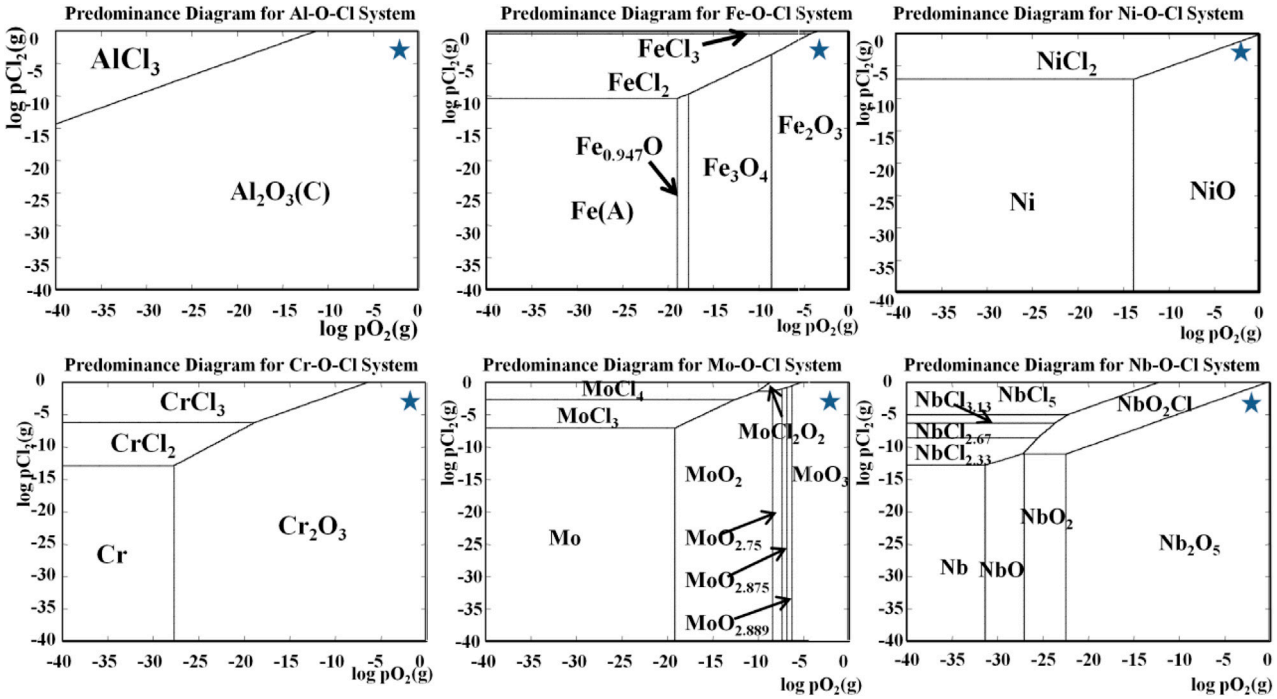


**FIGURE 13 |** Thermodynamic stability diagrams of the systems Nb–O–Cl, Fe–O–Cl, Al–O–Cl, Ni–O–Cl, Mo–O–Cl, and Cr–O–Cl at 800°C. The partial pressure of $O_2$ and HCl used in this study had been marked by "*".

oxide phases of the alloy elements could be predicted, which were mostly consistent with the XRD and SEM/EDS analysis as shown in **Figures 9**, **10**.

From the surface morphology and composition of alloys after high-temperature chloride corrosion at 700°C and 800°C for 55 h (**Figure 10**), it can be seen that, after corrosion at 700°C, the surface of the 904L sample consisted of two kinds of regions, one of which had a loose morphology, and the other had a flaky and cracked morphology. Combined with the XRD, SEM/EDS analysis, and the thermodynamic stability diagrams of the systems (**Figure 13**), it could be concluded that the former was composed of $Cr_2O_3$ and $Fe_3O_4$, and the latter was composed of $Cr_2O_3$ and $Cr_{1.3}Fe_{0.7}O_3$. Under the corrosion temperature of 700°C, the surface of the corroded AlFeNiMoNb plate showed gray, dark, and white areas. The gray area was composed of FeMoO, $Nb_2O_5$, $MoO_x$, and $Al_2O_3$. The dark area consisted of $NiAl_2O_4$, NiO, and a little $Fe_3O_4$. $MoO_x$ formed the principal phase of the white area. Because the driving force of Nb oxidation reaction is large, the formation of $Nb_2O_5$ is easier. At the same time, $Nb_2O_5$ has a high PBR value (2.68), and the volume of oxide is much larger than that of metal. The rapidly formed $Nb_2O_5$ cannot be completely spread on the surface but existed in the shape of flowering bread. For 904L: AlFeNiMoNb high-entropy alloy, the morphology of the corrosion layer after chloride corrosion at 700°C was similar to its metallographic structure. The gray area was composed of oxides of elements between dendrites, such as $Al_2O_3$, $Cr_2O_3$, $(Cr,Fe)_2O_3$, and $Fe_3O_4$. The dark area was mainly $Al_2O_3$, with a small amount of $Cr_2O_3$ and $(Cr,Fe)_2O_3$.

When the corrosion temperature was 800°C, the corrosion products on the surface of the 904L alloy showed obvious delamination. The outer layer was more compact, which was composed of $Fe_3O_4$. Deep cracks appeared in this outer layer. This cracking phenomenon led to the spallation of the corrosion products, thus, exposing the loose inner layer, which was composed of $Cr_2O_3$, $Fe_3O_4$, and NiO. For the AlFeNiMoNb plate, the thickness of the corrosion layer obtained after being corroded at 800°C was obviously larger than that at 700°C. The corrosion products were composed of a small area of dense $Al_2O_3$, a large area of $Fe_2O_3$, and protruding flower-like nodules. The nodules were mainly composed of Nb containing oxides such as $NiNb_2O_6$ and $Nb_2O_5$. $Fe_2O_3$ was also detected in this kind of region. When the corrosion temperature increased from 700°C to 800°C, the morphology of corrosion products on the surface of 904L:AlFeNiMoNb high-entropy alloy changed lightly, but the amount of corrosion products increased. As far as the composition was concerned, the content of $Al_2O_3$ in dendrites increased with the increase in temperature, while the content of $Cr_2O_3$ increased in inter-dendrites.

## Cross-Section Morphology and Composition of the Corroded Samples

**Figure 14** shows the cross-section morphology and composition of the samples corroded under $N_2$–2.6 vol.% $CO_2$–1.3 vol.% $O_2$–2,700 vppm HCl gaseous environment at 700°C and 800°C for 55 h. **Figures 15**, **16** show the element mapping of the cross-section of the corroded samples corroded under $N_2$–2.6 vol.%

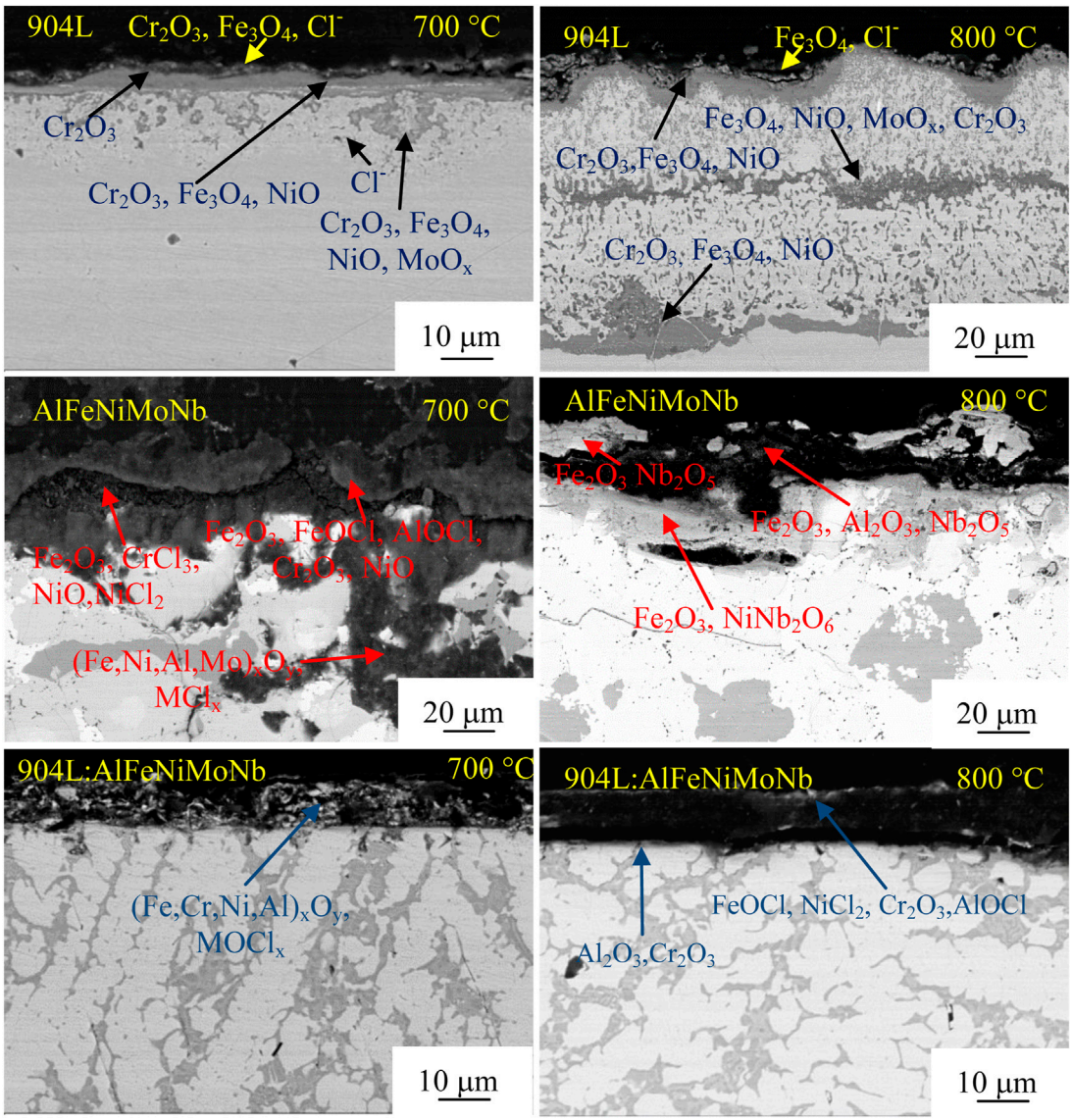


**FIGURE 14 |** Cross-section morphology and composition of the corroded samples corroded under $N_2$–2.6 vol.% $CO_2$–1.3 vol.% $O_2$–2,700 vppm HCl gaseous environment at 700°C and 800°C for 55 h.

$CO_2$–1.3 vol.% $O_2$–2,700 vppm HCl gaseous environment at 700°C and 800°C for 55 h.

After chloride corrosion at 700°C, the cross-section morphology of 904L showed that the corrosion products of the sample were mainly divided into three layers. The outermost layer was mainly composed of $Cr_2O_3$, a small amount of $Fe_3O_4$, and a trace amount of $FeCl_2$, which had a loose structure. The middle layer was composed of $Cr_2O_3$, $Fe_3O_4$, and NiO. Oxide of Mo appeared in the corrosion product layer near the substrate. Further to the interior of the matrix, there were more serious internal corrosion areas, and the main products were $Cr_2O_3$ and $Fe_3O_4$. At the same time, the Cl ion was detected in the internal corrosion zone. The loose oxides in the outer layer were formed by active oxidation in the process of high-temperature chloride corrosion, i.e., chloride ions reacted with metal oxides to obtain metal chlorides, which have a high vapor pressure. Metal chlorides were then oxidized to metal oxides again in the process of volatilization with the increase in the oxygen partial pressure. The oxides obtained by gas phase reaction were relatively loose and unprotected. The driving force of oxidation and chlorination reaction of Ni element was lower than that of other alloy elements. Therefore, the oxide of nickel grew slowly and was mainly located in the inner corrosion layer.

After chloride corrosion at 700°C, the corrosion layer of AlFeNiMoNb sample was thick, and serious internal corrosion occurred. At the same time, more corrosion spots can be found at the phase boundary. The corrosion layer was mainly oxides and

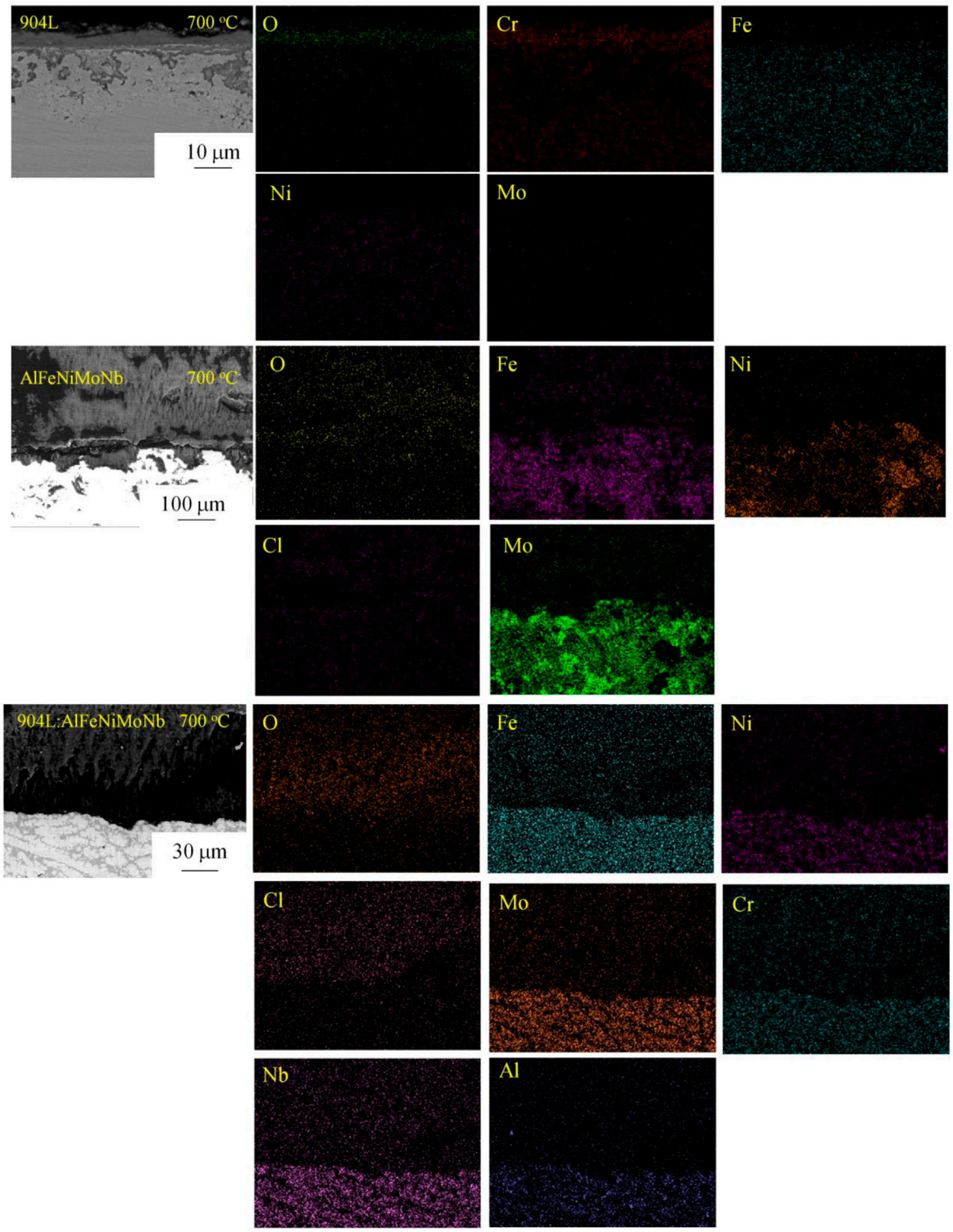


**FIGURE 15 |** Element mapping of the cross-section of the corroded samples corroded under $N_2$–2.6 vol.% $CO_2$–1.3 vol.% $O_2$–2,700 vppm HCl gaseous environment at 700°C for 55 h.

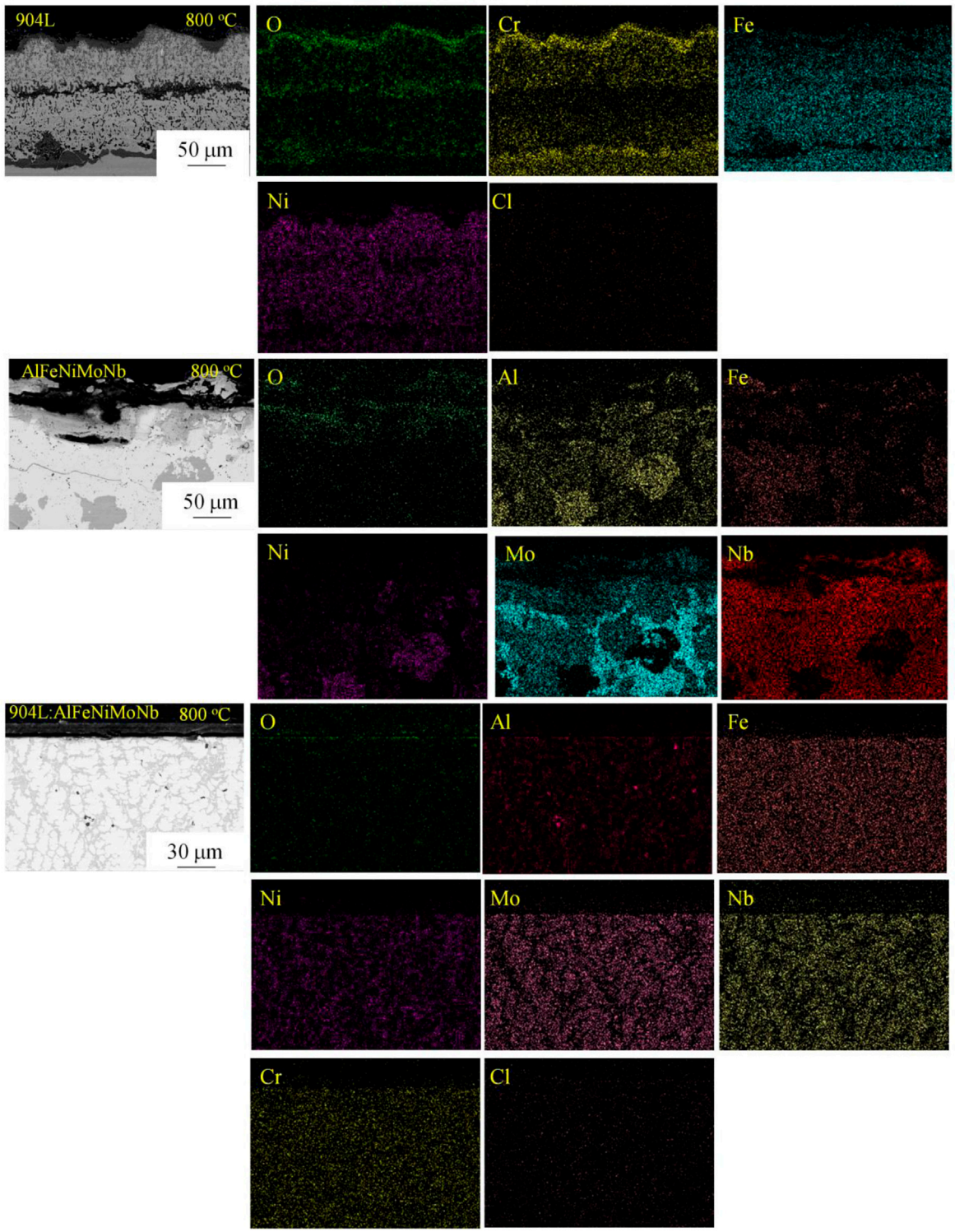


**FIGURE 16 |** Element mapping of the cross-section of the corroded samples corroded under $N_2$–2.6 vol.% $CO_2$–1.3 vol.% $O_2$–2,700 vppm HCl gaseous environment at 800°C for 55 h.

chlorine oxides of Fe, Cr, and Ni. When the corrosion layer was damaged, it was easy for the internal diffusion of corrosive element Cl to destroy the corrosion layer of metal oxides and form corresponding metal chlorides, such as $CrCl_3$ and $NiCl_2$, as shown in the figure. In the process of the outward diffusion of these chlorides, they were oxidized again to metal oxides with the increase in oxygen pressure. The metal oxides formed in this way had a loose structure, which could be seen in the middle of the corrosion layer shown in the figure. In the inner corrosion area, the main products were metal chlorides and oxides of Fe, Cr, Ni, and Al, in which the content of Fe was the highest.

For the 904L:AlFeNiMoNb sample, when being corroded under 700°C for 55 h, the sample obtained a simple corrosion layer, which was composed of $(Fe,Cr,Ni,Al)_xO_y$ and $MCl_x$. Although the corrosion layer was loose and broken, there was no inner oxidation found for this sample. The inner surface between the metal matrix and the corrosion layer was very flat, which indicated that the corrosion process of the sample was uniform. This uniform corrosion process was closely related to its uniform composition distribution and microstructure. Sluggish diffusion effect of high-entropy alloy could reduce the diffusion rate of corrosion elements in the 904L:AlFeNi-MoNb alloy, such as Cl and O elements. As a result, sluggish diffusion effect weakened the internal corrosion process, which could be seen in the actual situation that, although no continuous protective oxide layer was found, the Cl element was not detected under the corroded products near the matrix. These results mean that the sluggish diffusion effect of the 904L:AlFeNiMoNb high-entropy alloy plays a positive role in the resistance to high-temperature chloride corrosion.

When the corrosion temperature was raised to 800°C, the corrosion layer on the surface of the 904L alloy was thicker than that at 700°C. The outermost layer was iron oxide and metal chlorides, which had a broken appearance. Adjacent to this layer was a corrosion product region dominated by chromium oxide and containing part of iron oxide and nickel oxide. Continuing inward was an internal corrosion area with a certain depth. The second dark corrosion product layer appeared at half of the thickness of the whole corrosion layer. Combined with the EDS results and thermodynamic analysis, it was mainly the mixture of iron oxide, nickel oxide, molybdenum, and chromium oxide. Further inward, there was another internal corrosion area with nearly the same thickness as the front inner corrosion area. At the interface between the corrosion layer and the alloy matrix, it was a corrosion product layer dominated by chromium oxide and containing part of iron oxide and nickel oxide.

After chloride corrosion at 800°C, the chloride content in the corrosion layer on the surface of AlFeNiMoNb alloy was significantly lower than that at 700°C. The corrosion products were mainly composed of surface $Fe_2O_3$, $Nb_2O_5$, intermediate $Fe_2O_3$, $Al_2O_3$, and $Nb_2O_5$, as well as internal $Fe_2O_3$ and $NiNb_2O_6$. The corrosion along the phase boundary in the matrix was intensified.

For the 904:AlFeNiMoNb high-entropy alloy, after chloride corrosion at 800°C, the interface between the corrosion layer and the matrix was still relatively flat, indicating that the corrosion process was relatively uniform. Compared with the corrosion products at 700°C, the content of metal chloride oxides in the corrosion layer at 800°C increased, and they had loose microstructure and dark color in the SEM picture. The corrosion products with uniform thickness had poor adhesion to the alloy matrix. During the preparation of cross-section observation samples, the corrosion layer had been stripped from the matrix. On the surface of the substrate, there was a thin layer of corrosion product, which was the mixed oxides of $Al_2O_3$ and $Cr_2O_3$. These two oxides provide good shielding and protection for the high-temperature chloride corrosion of the alloy matrix.

The composition and the distribution properties of the corrosion products for 904L, AlFeNiMoNb, and 904L:AlFeNiMoNb high-entropy alloy were consistent with the analysis of the corrosion kinetics and the theoretical corrosion process mentioned above. The component selection and preparation of 904L:AlFeNiMoNb high-entropy alloy had achieved the expected experimental results. The existence of Al and Cr elements were conducive to the improvement of high-temperature chloride corrosion resistance of the alloy due to the formation of oxides that exist stably in chlorine-containing environment. At the same time, the dendrite structure of the uniform and refined high-entropy alloy kept the uniform and slow corrosion characteristics in the corrosion process, and there was no obvious internal corrosion. Thus, the destructive effect of Cl on the alloy matrix and oxide product layer was restrained to a great extent.

## CONCLUSION

1) To reduce the cost and improve the high-temperature chloride corrosion resistance, the 904L:AlFeNiMoNb high-entropy alloy was prepared by vacuum arc melting process. Corrosion tests of 904L, AlFeNiMoNb, and 904L:AlFeNiMoNb high-entropy alloy were carried out under $N_2$–2.6 vol.% $CO_2$–1.3 vol.% $O_2$–2,700 vppm HCl gaseous environment at 700°C and 800°C for 55 h.
2) Compared with 904L and AlFeNiMoNb alloys, 904L:AlFeNiMoNb high-entropy alloy had a rather homogeneous and refined dendrite microstructure. According to thermodynamic calculation and experiment results, the uniformly dispersed elements of Al, Cr, Ni, Mo, and Nb in the matrix will be conducive to the improvement of high-temperature chloride corrosion performance of the alloy. This prediction is consistent with the experimental results.
3) The 904L alloy was not suitable for application in an oxidizing chlorine-containing atmosphere above 700°C. The 904L:AlFeNiMoNb high-entropy alloy had the highest high-temperature chloride corrosion resistance among the tested samples at 700°C and 800°C, and also had the most stable corrosion characteristics with the change in temperature.

## DATA AVAILABILITY STATEMENT

The raw data supporting the conclusions of this article will be made available by the authors, without undue reservation.

## AUTHOR CONTRIBUTIONS

LB, WP, JX, XD: Investigation, Methodology, Writing-original draft, Software, Formal analysis. DM: Visualization, Data curation, Funding acquisition, JZ: Formal analysis, Visualization. XW: Writing - original draft. XS: Data curation. YW: Software. ZS: Resources. SY: Funding acquisition. XD: Conceptualization, Validation, Supervision, Writing - review and editing, Funding acquisition. XW: Validation, Supervision, Writing - review and editing. All authors listed have made a substantial, direct, and intellectual contribution to the work and approved it for publication.

## FUNDING

Financial support by the Science and Technology Research Program (GJJ190606) of Jiangxi Provincial Education Department of China is gratefully acknowledged.

## REFERENCES

Bender, R., and Schütze, M. (2003). The Role of Alloying Elements in Commercial Alloys for Corrosion Resistance in Oxidizing-Chloridizing Atmospheres. Part I: Literature Evaluation and Thermodynamic Calculations on Phase Stabilities. *Mater. corrosion* 54, 567–586. doi:10.1002/maco.200390129

Devendranath Ramkumar, K., Chandrasekhar, A., Srivastava, A., Preyas, H., Chandra, S., Dev, S., et al. (2016). Effects of Filler Metals on the Segregation, Mechanical Properties and Hot Corrosion Behaviour of Pulsed Current Gas Tungsten Arc Welded Super-austenitic Stainless Steel. *J. Manufacturing Process.* 24, 46–61. doi:10.1016/j.jmapro.2016.07.006

Devendranath Ramkumar, K., Chandrasekhar, A., Srivastava, A., Preyas, H., Chandra, S., Dev, S., et al. (2016). Effects of Filler Metals on the Segregation, Mechanical Properties and Hot Corrosion Behaviour of Pulsed Current Gas Tungsten Arc Welded Super-austenitic Stainless Steel. *J. Manufacturing Process.* 24, 46–61. doi:10.1016/j.jmapro.2016.07.006

Fantozzi, D., Matikainen, V., Uusitalo, M., Koivuluoto, H., and Vuoristo, P. (2017). Chlorine-induced High Temperature Corrosion of Inconel 625 Sprayed Coatings Deposited with Different thermal spray Techniques. *Surf. Coat. Tech.* 318, 233–243. doi:10.1016/j.surfcoat.2016.12.086

Galetz, B. R. A. M. (2017). Kinetics of Volatilization of High Temperature Corrosion Products and its Application to Chlorine Corrosion. *Mater. Corrosion* 68, 186–196. doi:10.1002/maco.201608841

Galetz, M. C., Rammer, B., and Schütze, M. (2015). Refractory Metals and Nickel in High Temperature Chlorine-Containing Environments - Thermodynamic Prediction of Volatile Corrosion Products and Surface Reaction Mechanisms: a Review. *Mater. Corrosion* 66, 1206–1214. doi:10.1002/maco.201408130

Gorr, B., Müller, F., Azim, M., Christ, H.-J., Müller, T., Chen, H., et al. (2017). High-Temperature Oxidation Behavior of Refractory High-Entropy Alloys: Effect of Alloy Composition. *OXID MET.* 88, 339–349. doi:10.1007/s11085-016-9696-y

Izzuddin, H., Hayashi, S., Yoneda, S., Kogin, T., Ishikawa, E., and Noguchi, M. (2020). Effect of Mo on Corrosion Behavior of Ni20Cr- X Mo Alloys in Air with NaCl-KCl-CaCl 2 Vapor at 570°C. *Mater. Corrosion* 71, 1488–1499. doi:10.1002/maco.201911469

Jia Chuntang. Research, S. M. L. S. (2019). Progress on Corrosion Performance of High Entropy Alloy Coatings. *Corrosion Sci. Prot. Technol.* 31, 343–348.

Lequien, F., and Moine, G. (2018). Corrosion of a 75Sn/25Pb Coating on a Low Carbon Steel in a Gaseous Environment Polluted with HCl: Mechanism. *Mater. Corrosion* 69, 1422–1430. doi:10.1002/maco.201810113

Li, L., Lu, J., Liu, X., Dong, T., Zhao, X., Yang, F., et al. (2021). Al CoCrFeNi High Entropy Alloys with superior Hot Corrosion Resistance to $Na_2SO_4$ + 25% NaCl at 900 °C. *Corrosion Sci.* 187, 109479. doi:10.1016/j.corsci.2021.109479

Li, Y. (2000). *Chlorination of Metallic Materials at High Temperature*. Corrosion Science and Protection Technology 12, 41–44.

Ma, W., Wenga, T., Frandsen, F. J., Yan, B., and Chen, G. (2020). The Fate of Chlorine during MSW Incineration: Vaporization, Transformation, Deposition, Corrosion and Remedies. *Prog. Energ. Combustion Sci.* 76, 100789. doi:10.1016/j.pecs.2019.100789

Pooja, M., Ravishankar, K. S., and Madav, V. (2021). High Temperature Corrosion Behaviour of Stainless Steels and Inconel625 in Hydroxide Salt. *Mater. Today Proc.* doi:10.1016/j.matpr.2021.02.266

Sadeghi, E., and Joshi, S. (2019). Chlorine-induced High-Temperature Corrosion and Erosion-Corrosion of HVAF and HVOF-Sprayed Amorphous Fe-Based Coatings. *Surf. Coat. Tech.* 371, 20–35. doi:10.1016/j.surfcoat.2019.01.080

Tsao, T., Yeh, A., Kuo, C., and Murakami, H. (2016). High Temperature Oxidation and Corrosion Properties of High Entropy Superalloys. *Entropy-Switz.* 18. doi:10.3390/e18020062

Viklund, P., Hjörnhede, A., Henderson, P., Stålenheim, A., and Pettersson, R. (2013). Corrosion of Superheater Materials in a Waste-To-Energy Plant. *Fuel Process. Tech.* 105, 106–112. doi:10.1016/j.fuproc.2011.06.017

Wang, J., Shi, W., Xiang, S., and Ballinger, R. G. Study of the Corrosion Behaviour of Sensitized 904L Austenitic Stainless Steel in Cl- Solution. *Corrosion Sci.* 181 (2021), 109234. doi:10.1016/j.corsci.2020.109234

Zahs, A., Spiegel, M., and Grabke, H. (1999). The Influence of Alloying Elements on the Chlorine-Induced High Temperature Corrosion of Fe-Cr Alloys in Oxidizing Atmospheres. *Mater. Corrosion* 50, 561–578. doi:10.1002/(sici)1521-4176(199910)50:10<561:aid-maco561>3.0.co;2-l

Zhang, W., Liaw, P. K., and Zhang, Y. (2018). Science and Technology in High-Entropy Alloys. *Sci. China Mater* 61, 2–22. doi:10.1007/s40843-017-9195-8

**Conflict of Interest:** The authors declare that the research was conducted in the absence of any commercial or financial relationships that could be construed as a potential conflict of interest.

**Publisher's Note:** All claims expressed in this article are solely those of the authors and do not necessarily represent those of their affiliated organizations, or those of the publisher, the editors and the reviewers. Any product that may be evaluated in this article, or claim that may be made by its manufacturer, is not guaranteed or endorsed by the publisher.